INSTITUTE OF PHYSICS PUBLISHING NANOTECHNOLOGY
Nanotechnology **16** (2005) 2153–2163 doi:10.1088/0957-4484/16/10/031

Investigation of single-walled carbon nanotube growth parameters using alcohol catalytic chemical vapour deposition

Husnu Emrah Unalan[1] **and Manish Chhowalla**

Rutgers University, Materials Science and Engineering, 607 Taylor Road, Piscataway, NJ 08854, USA

E-mail: unalan@rci.rutgers.edu

Received 17 March 2005, in final form 19 July 2005
Published 9 August 2005
Online at stacks.iop.org/Nano/16/2153

Abstract
A detailed parametric study of single-walled carbon nanotubes (SWNTs) synthesized in powder form and on substrates using the alcohol catalytic chemical vapour deposition (ACCVD) method is reported. As-grown SWNTs were analysed using transmission electron microscopy (TEM), field-emission scanning electron microscopy (FE-SEM), Raman spectroscopy and UV–vis–NIR spectroscopy to obtain structural and electronic information. We found that nucleation and growth of SWNTs occurs within seconds after introduction of the alcohol vapour and that high quality SWNTs with a narrow diameter distribution without amorphous carbon can be grown using Co acetate catalyst doped with Fe acetate above 750 °C. Defective multiwalled nanotubes were observed at lower temperatures, with the optimum temperature being 850 °C. These and other results reported in this paper allow the basis for optimizing the ACCVD process for the synthesis of large numbers of SWNTs.

(Some figures in this article are in colour only in the electronic version)

1. Introduction

The unique structural, mechanical and electrical properties [1–7] of single-wall carbon nanotubes (SWNTs) have rendered them appealing for investigations. The field of nanotube research is reaching maturity through demonstration of opto-electronic devices [8, 9], field effect transistors [10–12], and sensors [13–15]. Single-walled carbon nanotubes are synthesized by three primary methods: arc-discharge [16–18], laser ablation [19–21] and chemical vapour deposition [22–25]. Arc discharge and laser ablation produce SWNTs as powder samples in bundles while CVD offers synthesis of SWNTs on substrates [26–30] as well as in powder form [31, 32]. Additionally, using CVD one can control the diameter [33, 34], length and orientation [35, 36] of the nanotubes. Various CVD methods are now available for SWNT synthesis, including disproportionation of CO [37–39], high pressure catalytic decomposition of carbon monoxide (HiPCO) [40, 41] and the recently introduced alcohol catalytic chemical vapour deposition (ACCVD) [42–47]. In the ACCVD method developed by Maruyama *et al* [42], bimetallic Fe–Co nano-particles impregnated into zeolite supports are used as the catalysts and alcohol vapour is used as the carbon source to obtain SWNTs with high purity at 800 °C. The high purity is attributed to OH radicals associated with alcohols, which effectively removes the amorphous carbon during growth. This method is economical and offers advantages such as low synthesis temperature, simplicity and high yield as determined by a thermal gravimetric analyser (TGA) [43]. The ACCVD method was also used to synthesize SWNTs on substrates such as quartz, silicon [44, 46] and mesoporous silica [45]. Dip coating was utilized for loading catalyst

[1] Author to whom any correspondence should be addressed.

particles onto the substrates, and either randomly [44] or vertically aligned [46, 47] SWNTs were obtained. The vertically aligned SWNTs were obtained by utilizing a good background vacuum and low leak conditions. In addition to the work of Maruyama *et al*, alcohol vapour has also been shown to be an effective carbon source for synthesis of SWNTs by other groups [48–50]. Various apparatuses including hot filament assisted CVD [48] and cold wall CVD [49], both of which use a confined heating zone, have been used to synthesize SWNTs using alcohol vapours. In another system, laser ablation was used to vaporize a solid transition metal target, which was then used as the catalyst material for ACCVD [50]. In addition, SWNTs synthesized by ACCVD have been characterized using optical absorption spectroscopy in conjunction with Raman spectroscopy [51] and their chirality determined by fluorescence spectroscopy [52].

In this paper, we report on the growth of SWNTs using the ACCVD method. We have performed a detailed parametric study of the various factors influencing the growth of the carbon nanotubes. Specifically, we have investigated the effects of growth time and temperature, alcohol flow rate, type of alcohol (i.e. ethanol versus methanol) and catalyst concentration (Fe:Co acetate ratio) to further emphasize their effect on the properties of SWNTs. We have synthesized SWNTs in powder form on MgO support material and on substrates such as silicon and quartz. Our growth process consists of three stages: catalyst preparation, catalyst annealing and nanotube growth. The nanotubes are then characterized using field emission scanning electron microscopy (FE-SEM), transmission electron microscopy (TEM), Raman spectroscopy and UV–vis–NIR absorption spectroscopy.

2. Experimental details

The nanotubes were grown by the alcohol catalytic chemical vapour deposition method using a 2.54 cm quartz tube vacuum furnace. In the ACCVD method, alcohol vapour (either ethanol (bulk, purity = 95%) or methanol (Laboratory Grade, Fisher Scientific)) was used as the carbon source and metal acetates (mixture of Fe acetate (99.995%, Sigma-Aldrich) and Co acetate (99.999%, Sigma-Aldrich)) dissolved in deionized water (resistance = 15.6 Ω cm) or alcohol were used as the catalyst materials. The SWNTs were grown on a catalyst support bed (such as MgO (99.9%, Stanford Materials)) and on substrates (such as silicon (p-type (100)) and quartz (fused, Alfa Aesar)). Catalyst deposition was done in the following manner: 42 mg catalyst powder (iron acetate, cobalt acetate or a mixture of both) was bath sonicated in 10 ml of solvent (ethanol, methanol or DI water) for 15 min. For SWNT growth on MgO support material, 1.5 ml of this solution (6.3 mg solid loading) was drop cast onto a 200 mg MgO bed which was placed in an alumina combustion boat. Heating the catalyst mixture in a furnace to growth temperatures (450–950 °C) led to the elimination of the organic acetate layer, creating pure nano-sized catalyst particles which were used for the growth of SWNTs. A TEM image of the uniformly distributed nano-sized catalyst particles over a transparent portion of the MgO support material is given in figure 1. Higher contrast catalyst particles, indicated by arrows, can be seen on a thin section of MgO particles. The dip coating method was applied to

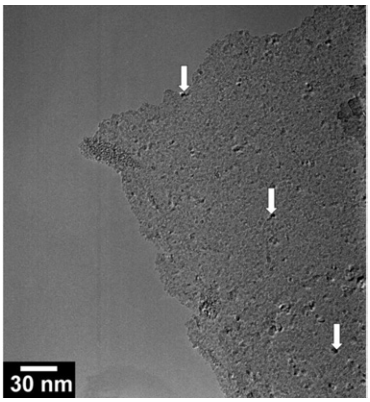

Figure 1. TEM image of the catalyst particles on a thin section of MgO support material.

substrates. In this method, substrates were dipped into the catalyst solution for 10 min, and then removed with a constant speed of 4 cm min^{-1} and allowed to dry in air for 5 min. Prior to dip coating, quartz and silicon substrates were cleaned by consecutive acetone and methanol sonication for 5 min, washed with DI water and blown with dry nitrogen. Quartz substrates were also annealed at 600 °C for 3 h prior to catalyst deposition in order to minimize stresses induced by cutting. The growth method was similar to the one described in [44] except for the H_2 reduction step during heating. MgO powder supported with catalyst particles was placed into alumina combustion boats, whereas a 10° inclined graphite stage was used to support the substrates. The chamber was first evacuated to 150 mTorr, and the samples were heated to the desired reaction temperature under 250 sccm of flowing argon. Once the growth temperature was reached (10–30 min depending on the growth temperature), the samples were held at that temperature for 5 min. The argon was then shut off and the tube was evacuated before the introduction of alcohol vapour. The alcohol vapour was then transferred into the quartz tube to achieve a pressure of 5–10 Torr. The alcohol flow rate in the growth chamber was controlled by controlling the bath temperature. After growth, the alcohol vapour was evacuated, argon was introduced and the reaction tube was cooled to room temperature. The SWNT growth time was kept constant at 20 and 50 min unless otherwise stated for SWNTs grown on MgO and substrate, respectively.

The SEM studies were performed on a LEO Zeiss Gemini 982 field emission scanning electron microscope operated at 5 kV. The TEM was performed on a TOPCON 002B ultra-high resolution transmission electron microscope operated at 200 kV in order to confirm the existence and morphology of the nanotubes. Nanotubes grown in powder form were sonicated in methanol and placed onto holey/lacey carbon coated copper grids for TEM observations, whereas SWNTs grown on quartz were transferred onto the grids by etching the quartz using $HF:HNO_3:H_2O$ (1:1:10) solution. As-grown samples were also analysed by a Renishaw System 1000 micro-Raman spectrometer using a laser wavelength of 785 nm. Raman spectroscopy was used to monitor the abundance, diameter distribution and purity of the nanotubes. Four different spectra were collected and averaged for accuracy. The

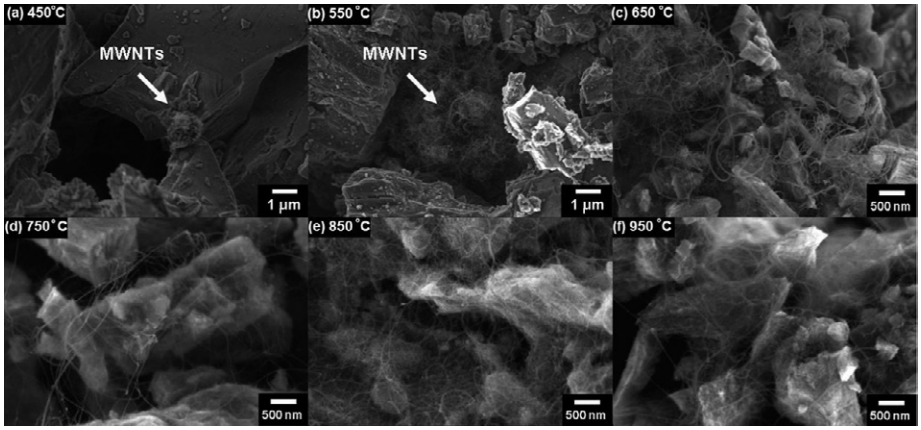

Figure 2. SEM images of nanotubes grown on MgO at (a) 450 °C, (b) 550 °C, (c) 650 °C, (d) 750 °C, (e) 850 °C and (f) 950 °C.

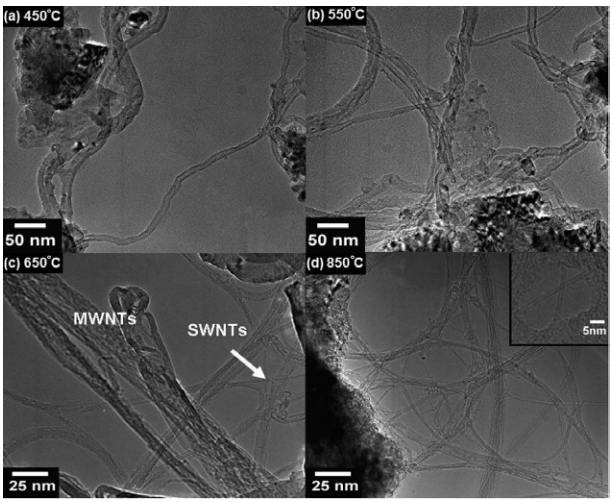

Figure 3. TEM images of nanotubes grown on MgO at (a) 450 °C, (b) 550 °C, (c) 650 °C and (d) 850 °C.

absorption was measured using a Perkin Elmer Lambda 9 UV–vis–NIR spectrometer with wavelengths in the 400–1600 nm range. As-grown quartz samples were used for absorption measurements [44]. The background obtained by measuring the absorption of catalyst loaded and annealed samples was subtracted from each measurement.

3. Results

3.1. Influence of growth temperature

Nanotubes were grown at six different deposition temperatures while keeping other variables such as growth time, alcohol flow rate and catalyst concentration constant. Ethanol was used as the carbon source. SEM images of the nanotubes grown on MgO at temperatures of 450, 550, 650, 750, 850 and 950 °C, respectively, are shown in figures 2(a)–(f). The TEM images of the nanotubes grown on MgO at temperatures of 450, 550, 650 and 850 °C, respectively, are shown in figures 3(a)–(d). The Raman spectra for the nanotubes grown at various temperatures are shown in figures 4(a) and (b). In order to compare the $I(\mathrm{D})/I(\mathrm{G})$ ratios, the spectra were normalized with respect to the G peak. It was found that nanotubes can be grown at temperatures as low as 450 °C (figure 2(a)). However, these nanotubes were observed to be multi-walled as seen in the TEM image given in figure 3(a). Raman spectra of the samples synthesized at 450 °C show a high intensity D peak which indicates the presence of highly defective structures and amorphous carbon [53]. At 550 °C, the number of nanotubes grown was found to increase significantly, but the high intensity D peak is also once again significant. The higher values of the D peak, indicative of disordered and amorphous carbon, can be attributed to non-optimized reaction conditions at low temperatures. The appearance of RBM peaks at 650 °C (figure 4(a)) indicates that the nucleation of SWNTs begins near this temperature. The presence of SWNTs at 650 °C was also confirmed with TEM (figure 3(c)) observations and is indicated by arrows. Our TEM observations indicate that nanotubes grown below 850 °C were found to be a mixture of SWNTs and MWNTs but the fraction of SWNTs increases dramatically with temperature, reaching ∼100% at 850 °C (figures 2(e), 3(d)). This indicates that the optimum growth temperature in our system is around 850 °C. Signatures of well crystallized SWNTs in the TEM, the presence of RBMs, the very small and broad D peak and the narrow and high intensity G peak with characteristic G splitting were observed for samples grown at 850 °C. Correlation between the SWNT diameter and RBM frequency was made using the empirical relationship $d = 248/\lambda$ [54, 55], where λ (cm^{-1}) indicates the RBM peak position and d (nm) the nanotube diameter. For all of our lower frequency Raman spectra, diameters of the SWNTs are given in the upper x-axis and were in good agreement with those obtained from TEM analysis (inset figure 3(d)). The purity of as-synthesized SWNTs was investigated by monitoring the intensity ratios of the Raman D to G peak [56, 57]. The $I(\mathrm{D})/I(\mathrm{G})$ ratio as a function of growth temperature is plotted in figure 4(c). It can be seen that above 650 °C the ratio decreases. At low temperatures, the D peak is prominent due to condensation of a-C and poorly crystallized NTs. At temperatures higher than 650 °C, the NTs are well crystallized and the $I(\mathrm{D})/I(\mathrm{G})$ ratio is significantly lower. The D peak, however, again begins to increase in intensity and broadens at 950 °C. As shown in figure 4(a), new peaks appear at lower Raman

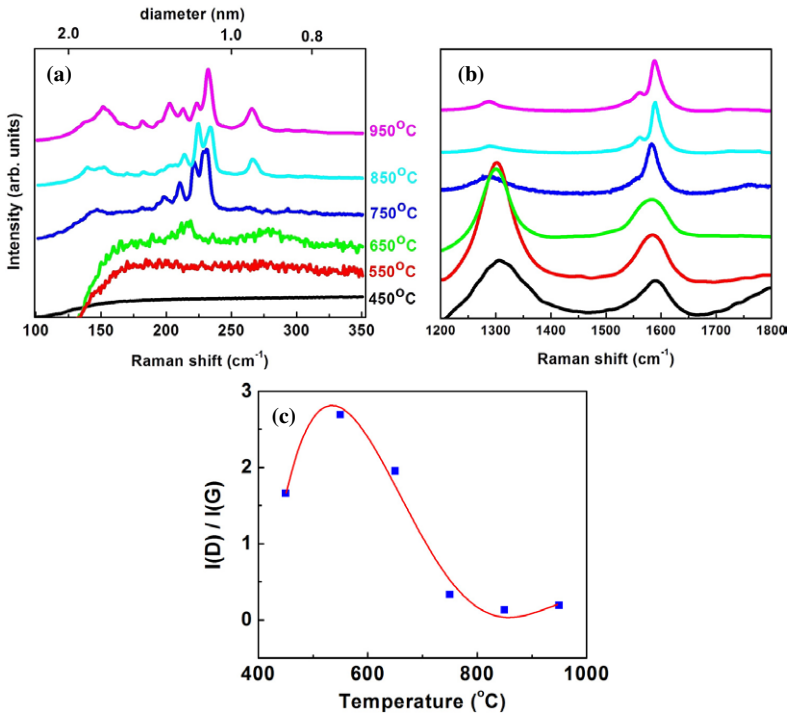

Figure 4. (a) Low frequency and (b) high frequency regions of the Raman spectra of nanotubes grown at various temperatures. (c) $I(\mathrm{D})/I(\mathrm{G})$ ratio with growth temperature.

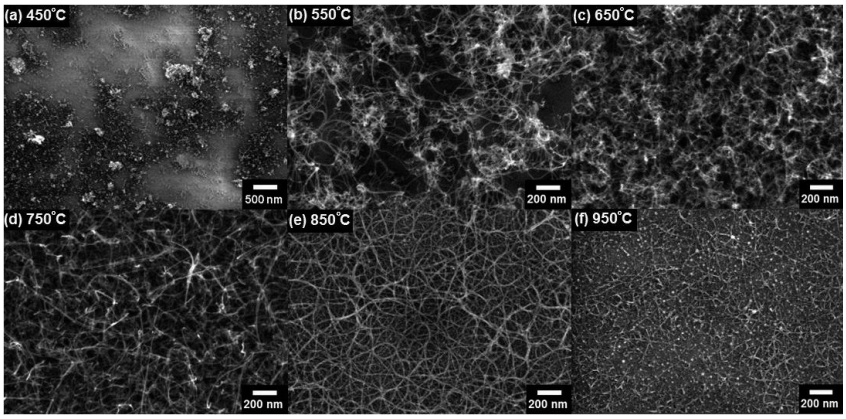

Figure 5. SEM images of nanotubes grown on quartz at (a) 450 °C, (b) 550 °C, (c) 650 °C, (d) 750 °C, (e) 850 °C and (f) 950 °C.

frequencies with growth temperature. This is attributed to the fact that larger diameter SWNTs are more stable at higher temperatures, while the smaller diameter SWNTs are less stable and are destroyed above the optimum temperature. The destruction of small diameter SWNTs in the form of amorphous or nano-crystalline carbon may explain the slightly higher $I(\mathrm{D})/I(\mathrm{G})$ ratio of the sample grown at 950 °C. In addition, enhancement in the $I(\mathrm{D})/I(\mathrm{G})$ ratio could also be explained by the thermal pyrolysis of ethanol to amorphous carbon at higher temperatures.

We have also investigated the feasibility of SWNT growth directly on substrates using the ACCVD method. The SEM images of the nanotubes grown on quartz substrates at temperatures 450, 550, 650, 750, 850 and 950 °C, respectively, are shown in figures 5(a)–(f). SWNTs on quartz are non-oriented and resemble 'spaghetti' type growth. Patchy growth was observed at 450 °C on quartz and the Raman results indicate the deposition of disordered carbon at that temperature. At 550 °C, few walled defective nanotubes were observed in the TEM as shown in figure 6(a). The threshold temperature for the presence of SWNTs was again found to be around 650 °C from Raman spectroscopy (figure 7(a)). Similar to growth on MgO, the optimum growth temperature was determined to be ∼850 °C (figures 5(e) and 6(b)) for the SWNTs grown on quartz. Raman spectra of SWNTs grown on quartz were similar to those grown on MgO, suggesting that the diameter distribution is comparable. Therefore, the type of substrate does not influence the diameter of the SWNTs, since the size of the catalyst particles is similar in both cases. The $I(\mathrm{D})/I(\mathrm{G})$ ratio is once again found to be a maximum

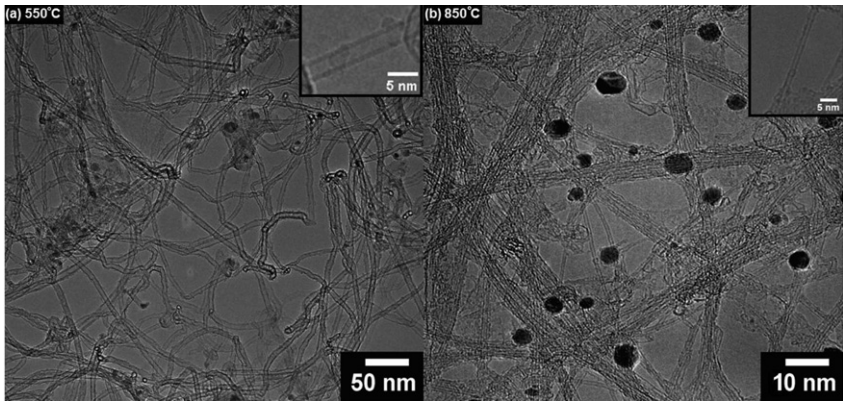

Figure 6. TEM images of nanotubes grown on quartz at (a) 550 °C and (b) 850 °C.

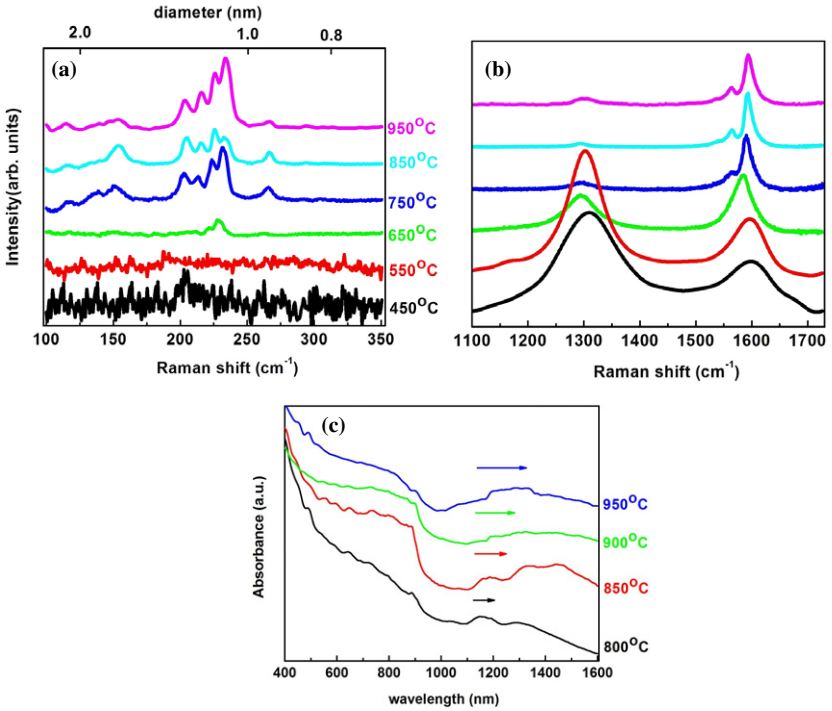

Figure 7. (a) Low frequency and (b) high frequency regions of the Raman spectra for nanotubes grown at various temperatures. (c) Optical absorption of as-grown SWNTs at various temperatures.

for nanotubes grown at 550 °C. This is attributed to the fact that at this temperature highly defective nanotubes are synthesized. In addition, we suspect that 650 °C may be an optimum temperature for cracking the alcohol vapour, lower than which leads to condensation of a large amount of amorphous carbon. Our results are in contrast to those of Maruyama *et al* [42], who found high purity SWNTs at temperatures as low as 550 °C. The cause of divergence of the results between our work and the data reported in [42] is unclear at present. However, differences in the experimental conditions such as the use of MgO as the catalyst bed instead of zeolites as well as the different flow rates and purity of alcohol may lead to different results.

The optical absorption spectrum of SWNTs is dominated by a series of sharp inter-band transitions (E_{11}, E_{22}, etc) associated with van Hove singularities due to their one-dimensional nature. The spectra consist of well resolved features from transitions between symmetrical van Hove singularities in the electronic density of states of both semiconducting and metallic SWNTs [58]. The optical absorption spectra of our SWNTs synthesized on quartz substrates are plotted in figure 7(c). The highest energy of transition was found to be 400–600 nm. We have found that the observed UV–vis–NIR spectra depend on the growth parameters. Samples grown at temperatures between 800 and 950 °C show well resolved absorption features, the one at 850 °C being the best. Our absorption peaks are not as sharp as those reported in [58], which we attribute to the presence of bundles of SWNTs and amorphous carbon. The presence of bundles leads to broadening of the electronic

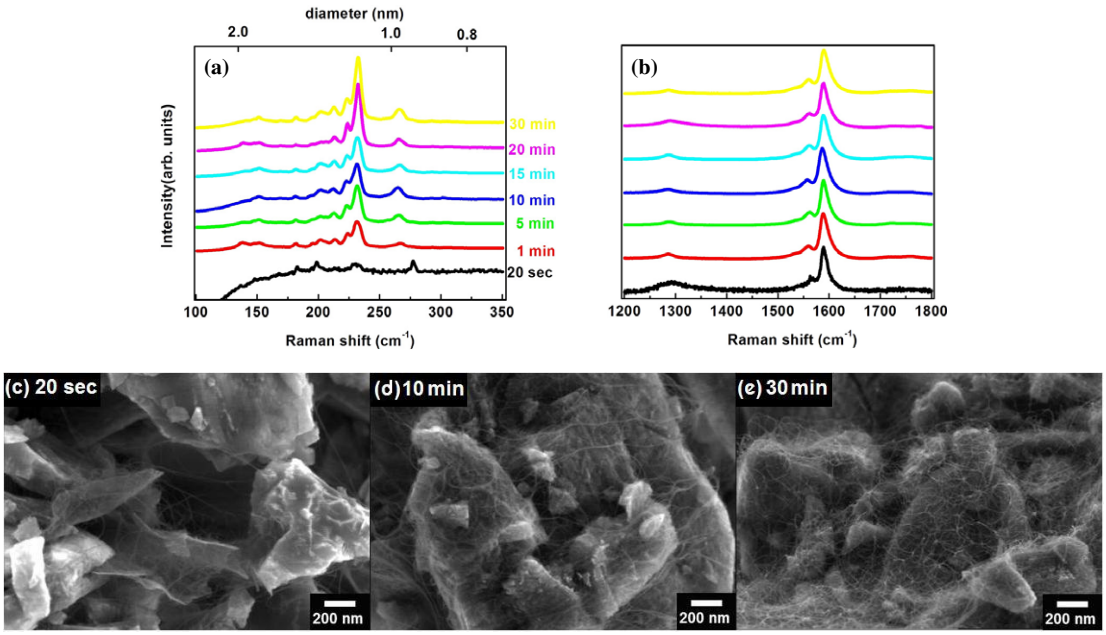

Figure 8. (a) Low frequency and (b) high frequency regions of the Raman spectra for SWNTs grown for different times. SEM images of SWNTs grown on MgO for (c) 20 s, (d) 10 min and (e) 30 min.

structure through van der Waals interaction between the SWNTs [59]. The amorphous carbon also has a detrimental effect because the van Hove singularities are effectively screened by the broad density of states background of the amorphous material. One can estimate the diameter of the SWNTs using the optical absorption data since the nanotube bandgap is roughly inversely proportional to their diameter [1]. In figure 7(c), a slight red shift was observed with an increase in growth temperature, which can be attributed to an increase in the mean diameter of the nanotubes (the magnitude of red shift is indicated by the length of the arrows as in figure 7(c)). This further supports the Raman results that the larger diameter SWNTs are found at temperatures >850 °C. Further information of the electronic structure of SWNTs would require dispersion and purification.

3.2. *Influence of growth time*

In order to investigate the time required for the nucleation and growth of SWNTs, we have varied the growth time while keeping all other parameters constant at the optimum values (T = 850 °C, alcohol flow rate = 8 ml min^{-1}, substrate = MgO). Ethanol was again used as the carbon source. The low and high frequency Raman spectra of SWNTs grown at different times are shown in figures 8(a) and (b), respectively. Our results indicate that there are no significant differences among the Raman spectra of SWNTs with deposition times. $I(\mathrm{D})/I(\mathrm{G})$ ratios remain nearly constant with growth time. Therefore, within the time period investigated, our results indicate that we have nearly amorphous carbon free SWNT growth with time. Twenty seconds was the minimum duration at which we were able to observe RBM features without luminescence from the background in the Raman spectra. Observing the low frequency region more closely, an increase in the area underneath the RBM peaks is seen with time. This can be attributed to continuous nucleation and growth of SWNTs with time. The overall increase in the quantity of the SWNTs with time was verified by SEM. The enhancement in the quantity of SWNTs on MgO can be clearly seen with time in figures 8(c)–(e). Numerous SEM images were taken to ensure that the images shown in figure 8 represent the evolution of SWNT growth with time. Continuous nucleation is only possible if there is no catalyst poisoning by amorphous carbon deposition. The $I(\mathrm{D})/I(\mathrm{G})$ ratio, in other words the quantity of amorphous carbon, was found to be constant up to 30 min of growth time. Nearly amorphous carbon free growth can be attributed to the OH radical associated with alcohols, which effectively removes disordered carbon during the SWNT growth [42], thereby preventing catalyst poisoning, enabling continuous nucleation. Longer growth times are currently under investigation in our laboratory.

3.3. *Influence of alcohol flow rate*

In order to investigate the influence of the amount of alcohol vapour in the reaction zone, we varied the alcohol flow rate. Ethanol was used as the carbon source. The alcohol flow rate was controlled by varying the temperature of the alcohol flask using a hot plate. The flow rate of the alcohol vapour into the quartz tube furnace as a function of the hot plate temperature is plotted in figure 9(a). Once again all other conditions such as growth temperature, time and preparation of catalyst were kept constant in order to study the influence of the alcohol flow rate. Our SEM observations of SWNTs grown at varying flow rates did not show any enhancement in production. Comparable yields of SWNTs can be explained by the equal amount of front exposed surfaces of the catalyst particles in different samples independent of the amount of carbon source. Our Raman spectra for low flow rates (<30 °C hot plate temperatures)

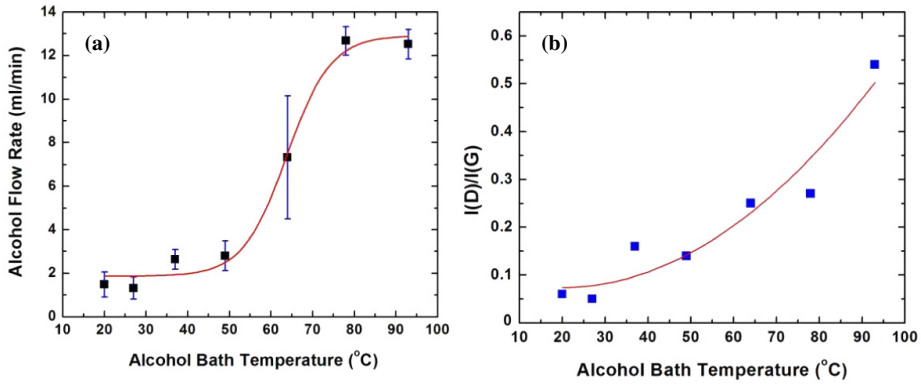

Figure 9. Variation of alcohol bath temperature versus (a) alcohol flow rate and (b) $I(\mathrm{D})/I(\mathrm{G})$ ratio.

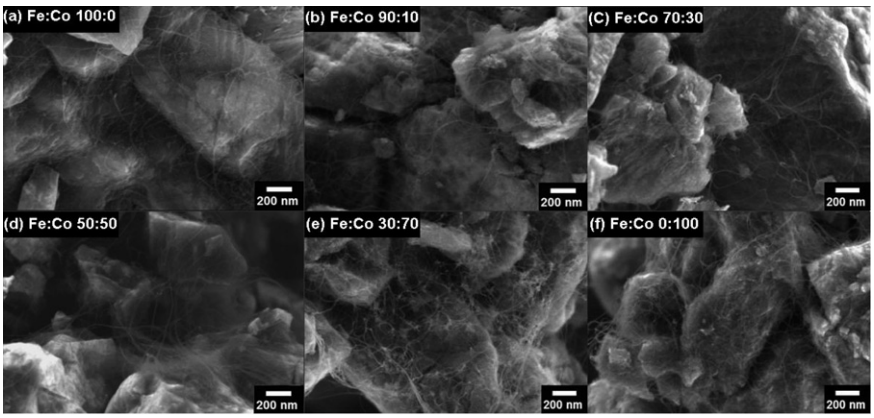

Figure 10. SEM images of SWNTs grown on MgO with Fe:Co ratios of (a) 100:0, (b) 90:10, (c) 70:30, (d) 50:50, (e) 30:70 and (f) 0:100, respectively.

resemble those of our optimized SWNTs. However, as the flow rate was increased, the amount of amorphous and disordered carbon was found to increase as indicated by the increase in the $I(\mathrm{D})/I(\mathrm{G})$ ratios plotted in figure 9(b). Therefore, instead of enhancing the number of SWNTs, the increase in alcohol concentration in the reaction chamber leads to production of disordered carbon. The formation of amorphous carbon may be attributed to three growth limiting mechanisms, which are catalyst poisoning, burning of SWNTs and impeded diffusion. Catalyst poisoning would stop SWNT growth by forming an amorphous carbon cage around the catalyst particle. Since we have similar yields at higher alcohol flow rates, catalyst poisoning is unlikely as previously discussed. On the other hand, burning of SWNTs can take place at higher temperatures and with high oxygen content. It is true that by increasing alcohol flow we are introducing more oxygen into the system, but since we have similar yields burning of SWNTs is not a significant factor. Following the catalytic decomposition of carbon feedstock at the catalyst surface, the reaction by-products must diffuse away so that the further reactions can continue. Diffusion of by-products (a-C in our case) will be obstructed by the increased alcohol molecules in the system. Therefore, the increase in the $I(\mathrm{D})/I(\mathrm{G})$ ratio can be attributed to the entrapment of a-C between the bundles of SWNTs with the increased alcohol flow rate.

3.4. Influence of catalyst concentration

In order to study the role of catalyst composition on the production of SWNTs, the Fe and Co acetate composition was varied while the total amount of the two was kept constant (42 mg). Ethanol was used as the carbon source and the growth temperature was 850 °C. The SEM images of the nanotubes grown on magnesium oxide with Fe:Co ratios of 100:0, 90:10, 70:30, 50:50, 30:70 and 0:100, respectively, are shown in images 10(a)–(f). The low and high frequency Raman spectra of SWNTs grown for different catalyst concentrations are shown in figures 11(a) and (b), respectively. Observing the low frequency region more closely, an increase in the area underneath the RBM peaks is seen with the increase in cobalt concentration. The increase in the RBM intensity associated with the increase in the quantity of the SWNTs can also be seen in the SEM images (figures 10(e) and (f)). The $I(\mathrm{D})/I(\mathrm{G})$ ratio is found to be high for the nanotubes grown with higher iron concentrations. This can be attributed to the deposition of more amorphous carbon at higher iron concentrations. The reason for this behaviour is unclear at present. Due to the absence of amorphous carbon and the high yield of SWNTs, cobalt rich concentrations were found to be optimum in the catalyst concentration study.

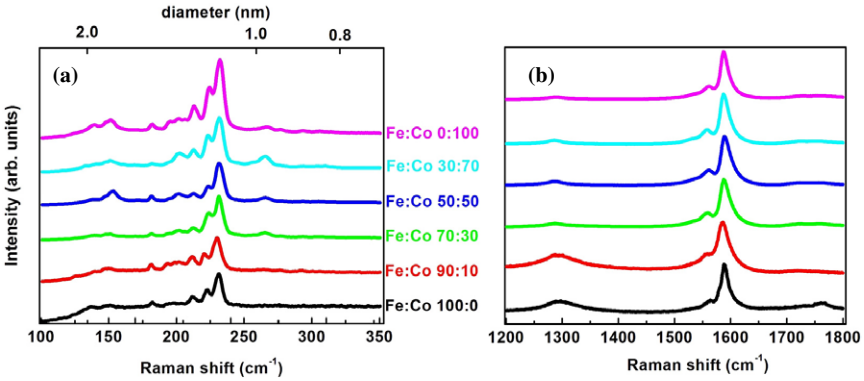

Figure 11. (a) Low frequency and (b) high frequency regions of the Raman spectra for SWNTs grown with different Fe:Co ratios.

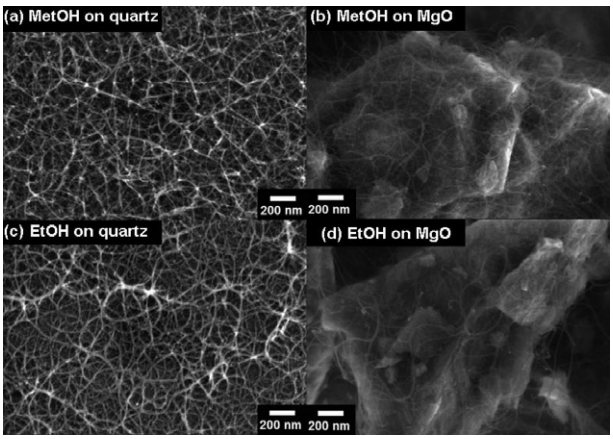

Figure 12. SEM images of the SWNTs grown using (a), (b) MetOH vapour and (c), (d) EtOH vapour on magnesium oxide support material and quartz substrates, respectively.

3.5. Influence of carbon source

Methanol was replaced with ethanol in order to monitor the effect of carbon source on the growth process. All other parameters such as furnace temperature, growth time and alcohol flow rate were kept constant. SEM images of the samples grown using methanol and ethanol vapour are shown in figure 12. SWNTs grown on quartz substrates and on MgO support showed an enhancement in the quantity when methanol vapour was used as a carbon source as shown in figure 12. The Raman spectra for the samples grown with methanol and ethanol vapour are shown in figures 13(a) and (b), respectively. The diameter distribution obtained from the lower frequency Raman data is similar for both samples except for larger diameter SWNTs. Samples grown with methanol vapour were found to contain a higher number of large diameter SWNTs. This is in contrast to the results of Maruyama *et al* [42], where methanol vapour was found to produce smaller sized bundles of SWNTs. In the high frequency Raman spectra, smaller and broader D peaks are observed when methanol vapour is used as the carbon source. This may be attributed to the more reactive nature of methanol compared to ethanol at the reaction temperature, thereby decreasing the quantity of deposited amorphous carbon. The optical absorption spectra of SWNTs synthesized with ethanol and methanol vapours are plotted in figure 13(c). Optical spectra are associated with a slight red shift for the nanotubes grown with methanol vapour, shown by the arrows in figure 13(c). Since nanotube diameter is inversely proportional to bandgap energies [1], this shift can be attributed to larger diameter of the nanotubes grown with methanol vapour, which further supports the Raman results. Unfortunately, direct comparison of methanol and ethanol cannot be carried out since experiments were conducted using different purity levels of alcohols and thus different water contents. The influence of the water may be significant during growth and thus it is being investigated in our laboratory. Nevertheless, our study provides a relative comparison between laboratory grade methanol and ethanol.

3.6. Influence of solvent used to dissolve catalyst particles

Ethanol, methanol and deionized water (DI) are used as three efficient solvents to dissolve the catalyst particles. No precipitation of catalyst was observed in any of the solvents after one hour of bath sonication. Pre-cleaned and annealed quartz substrates were dip coated in the catalyst solutions. In order to ensure that the deposition conditions were the same for all three samples, the growth was carried out simultaneously on all three samples. Ethanol was used as the carbon source and growth temperature was 850 °C. The SEM images of the SWNTs grown on quartz substrates with catalysts dissolved in the three different solvents are shown in figure 14. SWNT growth was found to be discontinuous on the quartz surface when alcohols were used as solvents, as shown in the inset. On the other hand, the better the wetting of the quartz surface by water[2] allows more uniform coating of the surface with the catalyst particles, which leads to more uniform growth of SWNTs. Therefore, we find that catalyst particles dissolved in DI water rather than ethanol or methanol lead to more uniform growth of SWNTs over the entire substrate surface. Investigation of SWNTs with Raman spectroscopy reveals similar characteristics as in our previous samples, as shown

[2] The surface tension equation can be written as $\gamma_{SV} = \gamma_{SL} + \gamma_{LV} \times \cos\delta$, where γ stands for surface tension and δ is called the dihedral angle. Complete wetting occurs when the drop spreads freely over the solid, which corresponds to the equation $\gamma_{SL} \leqslant \gamma_{SV} - \gamma_{LV}$, where S, L and V represent substrate, catalyst solution and air respectively in our system. Therefore, the modified surface tension balance is $\gamma_{quartz-solvent} \leqslant \gamma_{quartz-air} - \gamma_{solvent-air}$; the values are 22.1, 22.7, 72.8 nM m^{-1} for ethanol, methanol and deionized water, respectively.

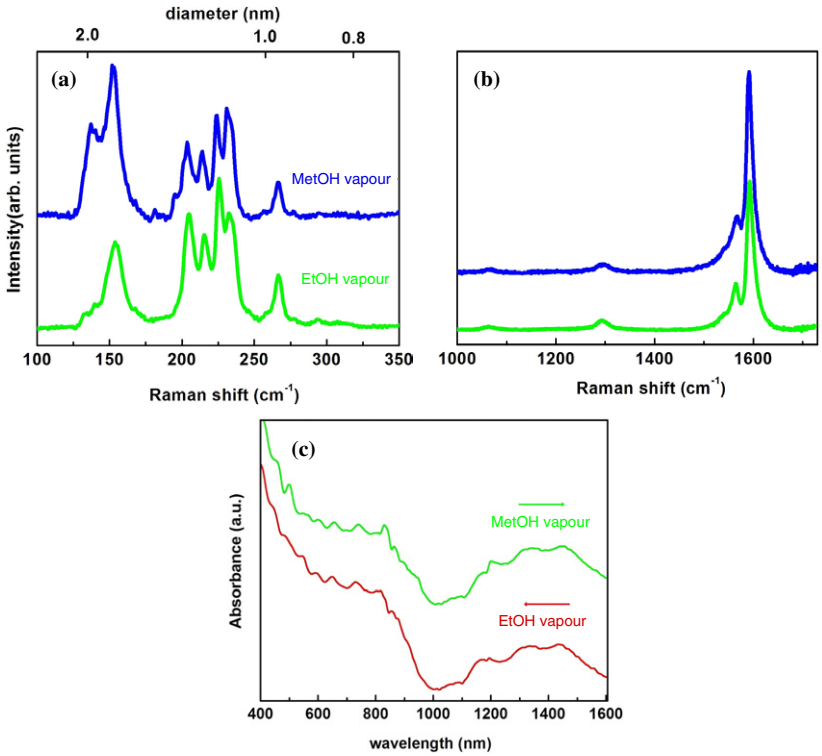

Figure 13. (a) Low frequency and (b) high frequency regions of the Raman spectra for SWNTs grown with ethanol and methanol vapour. (c) Optical absorption spectra of as-grown SWNTs using ethanol and methanol vapours.

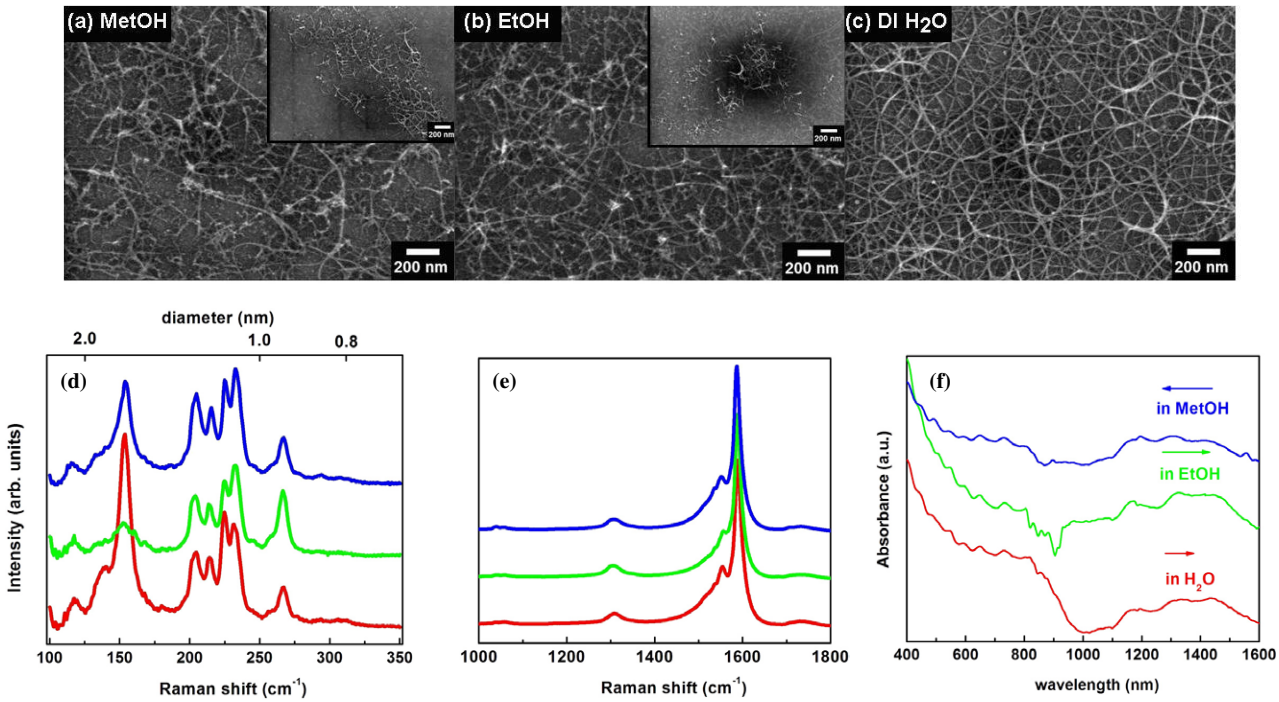

Figure 14. SEM images of the SWNTs grown using (a) MetOH, (b) EtOH and (c) DI water as a solvent for dissolving catalysts. (d) Low frequency and (e) high requency region of the Raman spectra for SWNTs grown with different solvents. (f) Optical absorption spectra of SWNTs grown with three different solvents used to dissolve the catalysts.

in figures 14(d) and (e). The diameter distribution was similar among those three samples, except for the large diameters. Since Raman wavelength is inversely proportional to diameter, the variation of the number of large diameter tubes with three different solvents is EtOH > DI water > MetOH. The reason for this behaviour is unknown since all three solutions were

clear after sonication and precipitation did not occur. Optical absorption data are given in figure 14(f). A slight red shift was observed for different solvents and its magnitude is indicated by the arrows given in the figure. Diameter information derived from optical absorption further supported the Raman results.

4. Conclusions

The process conditions for the growth of SWNTs using the ACCVD method was studied in detail as a function of growth temperature, time, alcohol flow rate, catalyst concentration, carbon source and solvent used to dissolve the catalyst particles. We used Raman spectroscopy to determine the onset of SWNT formation as well as to monitor the condensation of disordered carbon. Our results reveal that at growth temperatures $>$ 650 °C, RBMs from SWNTs are clearly visible and the intensity of the D peak is diminished up to 850 °C. Growth above this temperature (i.e. 950 °C) leads to de-stabilization of smaller diameter SWNTs, leaving behind larger diameter nanotubes and disordered carbon. This was also confirmed by UV–vis–NIR data, which showed a red shift with growth temperature, indicative of larger diameter nanotubes.

The use of methanol as the carbon source leads to an enhancement in the number of SWNTs. The amount of disordered carbon inferred from the Raman D peak was also found to be lower in methanol grown samples. Cobalt rich compositions were found to be better suited for optimized SWNTs in our process. Finally, catalyst dissolved in de-ionized water was found to provide uniform growth on substrates.

Acknowledgments

The authors would like to acknowledge the financial support from an NSF-ECS grant (0400501) and the US–Israel Binational Fund. We also acknowledge Professor Gene Hall (Rutgers University) for the use of the Raman instrument, and Dr Shashi Paul and Mr Alokik Kanwal for their help in this work.

References

[1] Dresselhaus M S, Dressselhaus G and Avouris Ph 2000 *Carbon Nanotubes, Synthesis, Structure, Properties, and Applications* (New York: Springer)
[2] Baughman R H, Zakhidov A A and de Heer W A 2002 *Science* **297** 787
[3] Iijima S and Ichihashi T 1993 *Nature* **363** 603
[4] Wong E W, Sheehan P E and Lieber C M 1997 *Science* **277** 1971
[5] Yu M F, Files B S, Arepalli S and Ruoff R S 2000 *Phys. Rev. Lett.* **84** 5552
[6] Odom T W, Huang J L, Kim P and Lieber C M 1998 *Nature* **391** 62
[7] Wildoer J W G, Venema L C, Rinzler A G, Smalley R E and Dekker C 1998 *Nature* **391** 59
[8] Baughman R H *et al* 1999 *Science* **284** 1340
[9] Star A, Lu Y, Bradley K and Gruner G 2004 *Nano Lett.* **4** 1587
[10] Tans S J, Verschueren A R M and Dekker C 1998 *Nature* **393** 49
[11] Collins P C, Arnold M S and Avouris P 2001 *Science* **292** 706
[12] Bachtold A, Hadley P, Nakanishi T and Dekker C 2001 *Science* **294** 1317
[13] Kong J, Franklin N R, Zhou C, Chapline M G, Peng S, Cho K and Dai H 2000 *Science* **287** 622
[14] Li J, Lu Y, Ye Q, Cinke M, Han J and Meyyapan M 2003 *Nano Lett.* **3** 929
[15] Novak J P, Snow E S, Houser E J, Park D, Stepnowski J L and McGill R A 2003 *Appl. Phys. Lett.* **83** 4026
[16] Bethune D S, Kiang C H, DeVries M S, Gorman G, Savoy R and Beyers R 1993 *Nature* **363** 605
[17] Journet C, Maser W K, Bernier P, Loiseau A, Lamy de la Chapelle M, Lefrant S, Deniard P, Lee R and Fischer J E 1997 *Nature* **388** 756
[18] Ebbesen T W and Ajayan P M 1992 *Nature* **358** 220
[19] Thess A *et al* 1996 *Science* **273** 483
[20] Guo T, Nikolaev P, Thess A, Colbert D T and Smalley R E 1995 *Chem. Phys. Lett.* **243** 49
[21] Yudasaka M, Komatsu T, Ichihashi T and Iijima S 1997 *Chem. Phys. Lett.* **278** 102
[22] Endo M, Takeuchi K, Kobori K, Takahashi K, Kroto H and Sarkar A 1995 *Carbon* **33** 873
[23] Kong J, Cassell A M and Dai H 1998 *Chem. Phys. Lett.* **292** 567
[24] Cassell A, Raymakers J, Kong J and Dai H 1999 *J. Phys. Chem.* **102** 6484
[25] Hafner J, Bronikowski M, Azamian B, Nikolaev P, Colbert D and Smalley R 1998 *Chem. Phys. Lett.* **296** 195
[26] Kong J, Soh H T, Cassell A, Quate C F and Dai H 1998 *Nature* **395** 878
[27] Franklin N R, Li Y, Chen R J, Javey A and Dai H 2001 *Appl. Phys. Lett.* **79** 4571
[28] Homma Y, Kobayashi Y, Ogino T and Yamashita T 2002 *Appl. Phys. Lett.* **81** 2261
[29] Seidel R, Liebau M, Duesberg G S, Kreupl F, Unger E, Graham A P, Hoenlein W and Pompe W 2003 *Nano Lett.* **3** 965
[30] Lacerda R G *et al* 2004 *Appl. Phys. Lett.* **84** 269
[31] Dai H, Rinzler G, Nikolaev P, Thess A, Colbert D T and Smalley R E 1996 *Chem. Phys. Lett.* **296** 471
[32] Nikolaev P, Bronikowski M J, Bradley R K, Rohmund F, Colbert D T, Smith K A and Smalley R E 1999 *Chem. Phys. Lett.* **313** 91
[33] Li Y M, Kim W, Zhang Y G, Rolandi M, Wang D W and Dai H J 2001 *J. Phys. Chem.* B **105** 11424
[34] Bachilo S M, Balzano L, Herrera J E, Pompeo F, Resasco D E and Weisman R B 2003 *J. Am. Chem. Soc.* **125** 11186
[35] Zhang Y G, Chang A L, Cao J, Wang Q, Kim W, Li Y M, Morris N, Yenilmez E, Kong J and Dai H J 2001 *Appl. Phys. Lett.* **79** 3155
[36] Huang S, Maynor B, Cai X and Liu J 2003 *Adv. Mater.* **15** 1651
[37] Alvarez W E, Kitinayan B, Borgna A and Resasco D E 2001 *Carbon* **39** 547
[38] Kitinayan B, Alvarez W E, Harwell J H and Resasco D E 2000 *Chem. Phys. Lett.* **317** 497
[39] Zheng B, Li Y and Liu J 2002 *Appl. Phys.* A **74** 345
[40] Nikolaev P, Bronikowski M J, Bradley R K, Rohmund F, Colbert D T, Smith K A and Smalley R E 1999 *Chem. Phys. Lett.* **313** 91
[41] Bronikowski M J, Willis P A, Colbert D T, Smith K A and Smalley R E 2001 *J. Vac. Sci. Technol.* A **19** 1800
[42] Maruyama S, Kojima R, Miyauchi Y, Chiashi S and Kohno M 2002 *Chem. Phys. Lett.* **360** 229
[43] Murakami Y, Miyauchi Y, Chiashi S and Maruyama S 2003 *Chem. Phys. Lett.* **374** 53
[44] Murakami Y, Miyauchi Y, Chiashi S and Maruyama S 2003 *Chem. Phys. Lett.* **377** 49
[45] Murakami Y, Yamakita S, Okubo T and Maruyama S 2003 *Chem. Phys. Lett.* **375** 393
[46] Murakami Y, Chiashi S, Miyauchi Y, Hu M, Ogura M, Okubo T and Maruyama S 2004 *Chem. Phys. Lett.* **385** 298

[47] Maruyama S, Einarsson E, Murakami Y and Edamura T 2005 *Chem. Phys. Lett.* **403** 320
[48] Okazaki T and Shinohara H 2003 *Chem. Phys. Lett.* **376** 606
[49] Chiashi S, Murakami Y, Miyauchi Y and Maruyama S 2004 *Chem. Phys. Lett.* **386** 89
[50] Nishide D, Kataura H, Suzuki S, Okubo O and Achiba Y 2004 *Chem. Phys. Lett.* **392** 309
[51] Maruyama S, Miyauchi Y, Murakami Y and Chiashi S 2003 *New J. Phys.* **5** 149.1
[52] Miyauchi Y, Chiashi S, Murakami Y, Hayashida Y and Maruyama S 2004 *Chem. Phys. Lett.* **387** 198
[53] Ferrari A C and Robertson J 2000 *Phys. Rev.* B **61** 14095
[54] Saito R, Dresselhaus G and Dresselhaus M S 2000 *Phys. Rev.* B **61** 2981
[55] Jorio A, Saito R, Hafner J H, Lieber C M, Hunter M, McClure T, Dresselhaus G and Dresselhaus M S 2001 *Phys. Rev. Lett.* **86** 1118
[56] Kataura H, Kumazawa Y, Maniwa Y, Otsuka Y, Sen R, Suzuki S and Achiba Y 2000 *Carbon* **38** 1691
[57] Holden J M, Zhou P, Bi X, Eklund P C, Bandow S, Jishi R A, Das Chowdhury K, Dresselhaus G and Dresselhaus M S 1994 *Chem. Phys. Lett.* **220** 186
[58] O'Connell M J *et al* 2002 *Science* **297** 593
[59] Reich S, Thomsen C and Ordejon P 2002 *Phys. Rev.* B **65** 155411